

Article

# CO and CO<sub>2</sub> Anode Gas Concentration at Lower Current Densities in Cryolite Melt

Nikolina Stanic <sup>1</sup>, Embla Tharaldsen Bø <sup>2</sup> and Espen Sandnes <sup>1,\*</sup>

<sup>1</sup> Department of Materials Science and Engineering, Norwegian University of Science and Technology NTNU, NO-7491 Trondheim, Norway; nikolina.stanic@ntnu.no

<sup>2</sup> SINTEF Helgeland AS, Nytorget 5, 8622 Mo i Rana, Norway; embla.tharaldsen@sintef.no

\* Correspondence: espen.sandnes@ntnu.no; Tel.: +47-48606478

Received: 9 November 2020; Accepted: 15 December 2020; Published: 20 December 2020



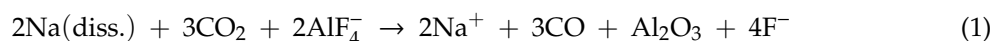
**Abstract:** This work aims to study the CO-CO<sub>2</sub> gas composition at low potentials and low current densities in cryolite melt with relatively low alumina content (≤2 wt%). There is a scarcity of data in the literature regarding the low current density region and also for bath low in alumina. The experimental setup was constructed to minimize the back reaction as well as the Boudouard reaction. For potentials up to 1.55 V and corresponding current densities up to 0.07 A cm<sup>-2</sup>, it was found that CO is the dominant product. Between 1.55 and 1.65 V (corresponding current density region 0.07 to 0.2 A cm<sup>-2</sup>), CO<sub>2</sub> becomes the dominant gas product. These potential values are probably slightly large due to suspected Boudouard reaction between CO<sub>2</sub> and carbon particles in the melt formed by disintegration of the graphite anode. The results are discussed in relation to the literature data and thermodynamic calculations.

**Keywords:** aluminum electrolysis; graphite anodes; CO-CO<sub>2</sub> gas analysis; carbon consumption

## 1. Introduction

The electrochemical anode gas product in industrial aluminum electrolysis is CO<sub>2</sub>, but also some CO is produced electrochemically. The amount of electrochemically produced CO is difficult to determine since there are several chemical reactions where CO<sub>2</sub> is converted to CO. The electrochemically produced compounds are termed primary products and chemically produced compounds are termed secondary products.

The anode gas from the industrial cells contains a considerable amount of CO, where most of the CO is formed by the back reaction between dissolved anodic and cathodic products, CO<sub>2</sub> (diss.) and Al (diss.), respectively. Aluminum mainly dissolves in the bath through reaction with sodium fluoride, forming dissolved sodium, Na (diss.), and aluminum fluoride. The nature of the dissolved aluminum is still not completely resolved, and in the industrial electrolyte composition, sodium-containing species are dominant. Sodium dissolves in the electrolyte in the form of free Na, while dissolved aluminum is probably present as the monovalent species AlF<sub>2</sub><sup>-</sup>, which, by anodic oxidation, becomes AlF<sub>4</sub><sup>-</sup>. A suggested back reaction takes the form [1]:



The current efficiency in the industry has improved over the years. For example, in terms of gas measurements, Thonstad reported in 1964 [2] that the industrial anode off-gas consists of CO<sub>2</sub> together with 30–50% of CO. Kimmerle and Noël observed in 1997 [3] 82% CO<sub>2</sub> and 17% CO in industrial anode off-gas. Aarhaug et al. reported in 2016 [4] 7700 ppm of CO<sub>2</sub> and 764 ppm CO in off-gas from primary aluminum production, which would correspond to around 9% of CO and 91% of CO<sub>2</sub>.

Another possibility for forming CO is through the Boudouard reaction:



CO<sub>2</sub> gas reacts with solid carbon, forming CO gas. In Figure 1, the equilibrium pressures of CO and CO<sub>2</sub> at a total pressure of 1 atm for reaction 2 are shown. Above 950 °C, CO is the dominant product.

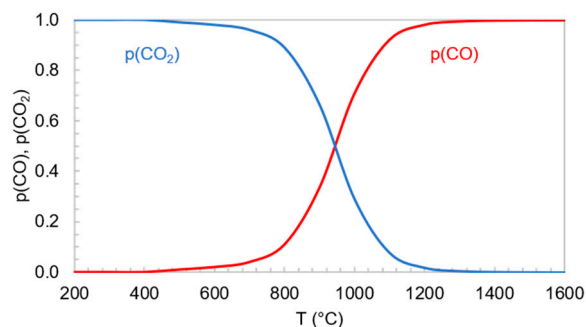
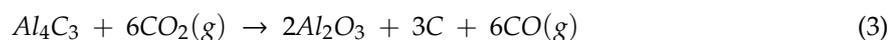


**Figure 1.** Temperature-dependent equilibrium of the Boudouard reaction.

The carbon reacting in reaction 2 may be anode carbon or carbon particles floating in the bath formed by disintegration (dusting) of the carbon anodes during electrolysis. Reaction 2 most likely occurs on the melt surface, where carbon particles are concentrated. Thonstad [5] studied the anode process during aluminum electrolysis in the laboratory-scale cell. In that study, the reaction between CO<sub>2</sub> and carbon particles was studied by the addition of carbon particles to the melt using a non-disintegrating anode. It was observed that CO<sub>2</sub> reacted with the carbon particles to form CO (reaction 2). The non-disintegrating anode, i.e., a carbon anode made with the addition of some chemicals that make the carbon anode less reactive, was used in order to test if CO<sub>2</sub> can react with the anode itself. For this experiment, CO<sub>2</sub> was bubbled under the anode. It was found that CO<sub>2</sub> cannot react with the anode at normal current densities. It was concluded that the positive surface charge of the anode which is in contact with the bath is the reason for its non-reactivity to CO<sub>2</sub>. Barrillon found that the outer surface layer is more porous than the interior layer of the anode [6]. Carbon atoms within such pores are non-polarized as they are not in contact with the bath. Although Thonstad found that CO<sub>2</sub> cannot react with the anode itself, gas might penetrate into cracks and pores in the anode and the Boudouard reaction can take place there.

Ouzilleau et al. [7] proposed an electrothermodynamic model for the carbon anode consumption of the prebaked carbon anodes in the aluminum electrolysis process for the prediction of CO<sub>2</sub>-CO emission ratios. Their model predicts trends of some operating parameters on the CO<sub>2</sub>-CO ratio in the primary anode gas; an increase in anodic interface potential E increases the CO<sub>2</sub>-CO ratio, an increase in carbon anode baking temperature increases the CO<sub>2</sub>-CO ratio, and an increase in the operating electrolysis temperature decreases CO<sub>2</sub>-CO ratio. The model predicts that polarized coke crystallinities preferentially form CO<sub>2</sub> during electrolysis and dispersed, non-polarized, carbon particles would rather react with CO<sub>2</sub> to form CO (reaction 2). Another secondary reaction is the formation of CO by the reaction of the primary anode gas and non-polarized carbon atoms within pores in the interior of the carbon anode following the penetration of CO<sub>2</sub> in the non-polarized structure as mentioned above.

Another source of CO could be the anodic oxidation of aluminum carbide, where carbon dust is also formed [8]:



In the present work, the laboratory cell setup was constructed in a such way that anodic and cathodic areas were physically separated in order to limit the reaction between anodic and cathodic products. Thus, reaction 1 and reaction 3 can be considered to contribute negligibly to the CO<sub>2</sub>

conversion. CO can also be formed by air burn. Since nitrogen is flushed through the furnace, air burn in the laboratory-scale cell could also be neglected.

Thorne et al. [9] used GC MS to measure CO and CO<sub>2</sub> based on an adapted method from Kjos et al. [10], who used anodes with a hole in the center for the gas collection. Thorne et al. found that the main product was CO<sub>2</sub> but substantial amounts of CO were also detected. The CO was proposed to originate mostly from the back reaction, but CO was also proposed to partially be a primary anode product or formed via the Boudouard reaction. Grjotheim et al. [11] measured the anode gas composition as a function of the anodic current density and found close to 100% of CO<sub>2</sub> in the current range 0.32–1.34 A cm<sup>-2</sup>. The hollow anode applied was designed to effectively collect the gases after being formed without coming into contact with the outer bath surface. A hole was made through the center of the anode for gas collection. For graphite, it was found that the anode consumption was much higher (in the range 135–150%) than the theoretical value. For the analysis of the anode gas during electrolysis in a bath with low alumina concentration (<0.6 wt%), Zhu and Sadoway [12] used a tubular anode where the outer vertical surface was insulated with boron nitride to avoid contact with the electrolyte. It was found that over the entire potential range, CO was the main component of the anode gas. Brun et al. [13] studied the Boudouard equilibrium in a laboratory-scale aluminum cell and found that carbon particles probably formed by disintegration of the anode could react with the CO<sub>2</sub>, causing its reduction to CO.

Most of the experiments for studying CO-CO<sub>2</sub> composition are performed at higher current densities [9,11,14]. Clearly, CO<sub>2</sub> seems to be the primary anodic off-gas. However, there is a scarcity of studies at lower current densities where also CO could be the primary off-gas. This work aims to study more closely the CO-CO<sub>2</sub> composition at low potentials and the corresponding low current densities and to thoroughly discuss the obtained results in relation to the few literature references that exist. Drossbach [15], Thonstad [5] and Silny and Utigard [16] have reported gas composition data for low current densities but also as well for higher current densities. Only in the work by Thonstad, CO was found to be the dominant product at a potential close to the reversible potential for CO evolution. The present work aims to contribute to the fundamental understanding of CO-CO<sub>2</sub> gas composition at lower potentials and current densities. The study was conducted in a laboratory cell where also different anode designs were used. The different designs were introduced because they could potentially give different gas compositions. Four different anode designs were used: horizontal anode (with a downward-facing surface), vertical anode, rod anode (having both a vertical and horizontal surface) and an inverted horizontal anode (with an upward-facing surface). The carbon material used was graphite. The bubble behavior of these electrodes has been reported in an earlier paper [17]. A hollow anode design made from the same graphite material was also tested.

## 2. Materials and Methods

Experiments were performed in a cryolite melt (cryolite ratio = 3) under N<sub>2</sub> atmosphere at the temperature of 1005 °C. Nitrogen also had a role as a carrier gas. Synthetic cryolite (purity ≥ 97.0%, Sigma Aldrich) was used. Alumina (Merck) was added to the cryolite to produce a start concentration of 2 wt% of alumina. The different anode designs are shown in Figure 2. The graphite rod anode was produced as described in [9]; the vertical anode, horizontal anode and inverted horizontal anode together with the counter electrode (CE) were produced as described in [17]. As a counter electrode (CE), a graphite rod shielded with boron nitride was used. The surface area was 10.2 cm<sup>2</sup>. The purpose of shielding the CE was to minimize the exposed carbon above the melt. The CE was physically separated from the anode by placing it in a smaller silicon-nitride crucible, thus preventing cathodic and anodic products from reacting. The hollow gas anode had the shape of an inverted funnel and was designed as shown in Figure 3. The force for driving the anode gas out of the cell was the overpressure made by the produced gas, i.e., no carrier gas was used. When the hollow anode was used as the working electrode, the graphite crucible had a role as counter electrode. A purified graphite

material (Schunk Tokai Scandinavia, AB, Sweden) was the active electrode material for all electrodes. The aluminum reference electrode was constructed according to [10].

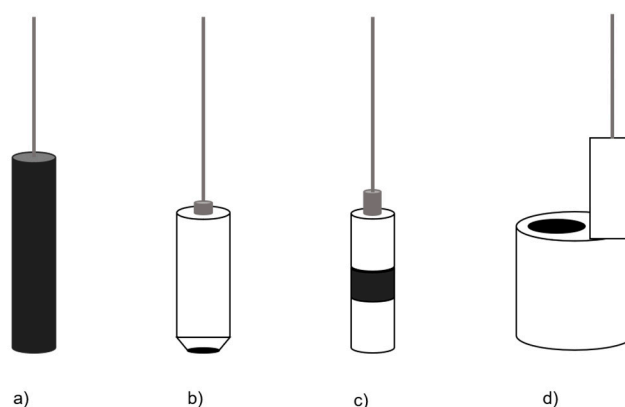


**Figure 2.** Different anode designs: (a) rod anode, when immersed 10 mm in melt gives a geometric surface area of approx.  $3.9 \text{ cm}^2$ , (b) horizontal anode, anode surface area  $0.79 \text{ cm}^2$ , (c) vertical anode, anode surface area  $1.57 \text{ cm}^2$ , (d) inverted horizontal anode, anode surface area  $0.69 \text{ cm}^2$ .

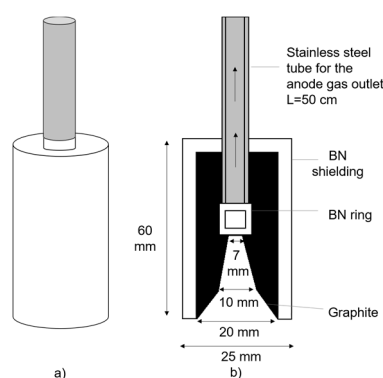


**Figure 3.** The hollow gas anode; (a) the outer body of the hollow gas anode, (b) cross-section of the hollow anode design with the inverted funnel shape, anode surface area approx.  $10.8 \text{ cm}^2$ .

Three cell setups were used in this work; see Figure 4. In order to study the  $\text{CO}_2$  to  $\text{CO}$  conversion through Boudouard reaction for Setup 1 and Setup 2, a known concentration (1% and 2%) of  $\text{CO}$  and  $\text{CO}_2$  was introduced for a certain amount of time without electrolysis at a working temperature of  $1005 \text{ }^\circ\text{C}$  while analyzing the composition of the out gas. Setup 1 was expected to have a high degree of conversion due to the graphite crucible and therefore Setup 2 with a silicon nitride ( $\text{Si}_3\text{N}_4$ ) crucible was introduced to minimize any reaction between  $\text{CO}_2$  and carbon. The anode and cathode were physically separated in order to prevent anodic and cathodic products from reacting (reaction 1). The counter electrode was placed inside a smaller silicon-nitride crucible. This was done to minimize the back reaction by preventing the transport of dissolved aluminum metal from the cathode compartment to the anode compartment. Three small holes were drilled in the small  $\text{Si}_3\text{N}_4$  crucible to ensure ionic contact between the compartments. The gas was collected by a hollow steel tube above the bath surface near the anode. Setup 2 was used to study the gas composition of the four anode designs shown in Figure 2. It was also tested for  $\text{CO}_2$  to  $\text{CO}$  conversion in the same way as Setup 1. The degree of conversion was relatively small and considerably smaller than for Setup 1. Obtained results were used for correction of measured gas concentration values for the four different anodes tested using Setup 2. Setup 3 (shown in Figure 4c) was used for the gas measurements with the hollow gas anode. The BN ring (shown in Figure 3b) was inserted to prevent the stainless steel tube from coming into direct contact with the melt. The graphite crucible was used as a counter electrode.

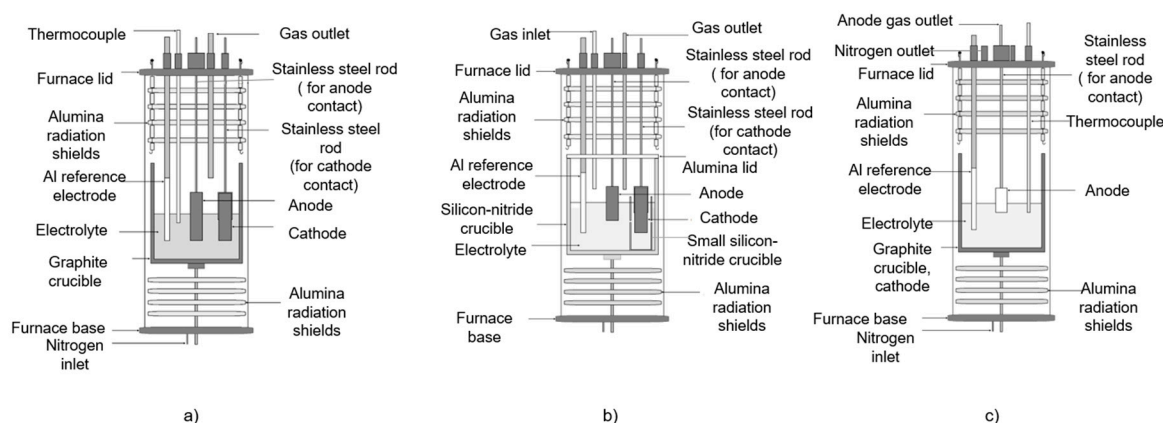


Figure 4. The three different setups: (a) Setup 1, (b) Setup 2, (c) Setup 3.

Electrochemical impedance spectroscopy (EIS) was used to determine the ohmic resistance at open circuit potential (OCP). This value was used to IR compensate all electrochemical measurements. This means that any voltage drop due to resistance introduced by bubbles and overvoltage has not been compensated. Chronoamperometry was used for the potential control of the working electrode. The potential of the working electrode was kept constant for  $> 300$  s and the resulting current was monitored for several potentials. The current density was corrected for the change in the anode surface area due to carbon consumption (this only applies to the rod and vertical anode). The corresponding gas concentration was measured continuously. A minimum time of 300 s was needed for the gas concentration to stabilize. For the hollow gas anode, chronopotentiometry was used. All electrochemical measurements were performed using a PARSTAT (Princeton Applied Research, potentiostat and a 20 A booster (KEPCO).

A gas analyzer (Servomex Xendox 2550 Multicomponent Infrared) was used to analyze the concentration of the CO and CO<sub>2</sub>. The gas analyzer yielded potential values proportional to the gas concentration in vol%. A calibration was done before each experiment and calibration curves were constructed for both CO and CO<sub>2</sub>, giving the relation between output potential and gas concentration in vol%. For the gas measurements, the gas flow was kept constant at 400 mL/min and the flow was controlled with a flow meter (Bronkhorst mass flow meter/controller).

### 3. Results and Discussion

#### 3.1. Testing of Setup 1 and Setup 2 for CO<sub>2</sub> to CO Conversion

Setup 1 and Setup 2 were studied for CO<sub>2</sub> to CO conversion and the results were used for correcting the gas measurement values obtained for the anode testing. Results are shown in Figures 5 and 6 for Setup 1 and Setup 2, respectively. For Setup 1, the CO(1%)/CO<sub>2</sub>(2%)/N<sub>2</sub>(balance) gas mixture was introduced at the bottom of the furnace and passed on the outside of the graphite crucible on its way through the furnace. Figure 5 shows a considerable decrease in CO<sub>2</sub> and increase in CO concentration, indicating significant CO<sub>2</sub> conversion to CO. When the gas mixture was flushed directly through the analyzer, the actual concentration of the CO and CO<sub>2</sub> in the gas mixture was measured. Pure nitrogen gas was flushed through the analyzer and the furnace before and after the introduction of the gas mixture. When nitrogen was flushed through the furnace, considerable CO concentration was obtained while CO<sub>2</sub> reached zero value. This CO excess could be caused by traces of O<sub>2</sub> in N<sub>2</sub> gas reacting with carbonaceous material in the furnace. However, the purity of the N<sub>2</sub> gas was 99.999% and could not cause significantly high values of CO. The cause of the high CO value is not understood, but this phenomenon was not observed for Setup 2. The gas mixture was then introduced to the furnace with an arbitrary sequence of flow rate and the CO and CO<sub>2</sub> concentrations were measured.

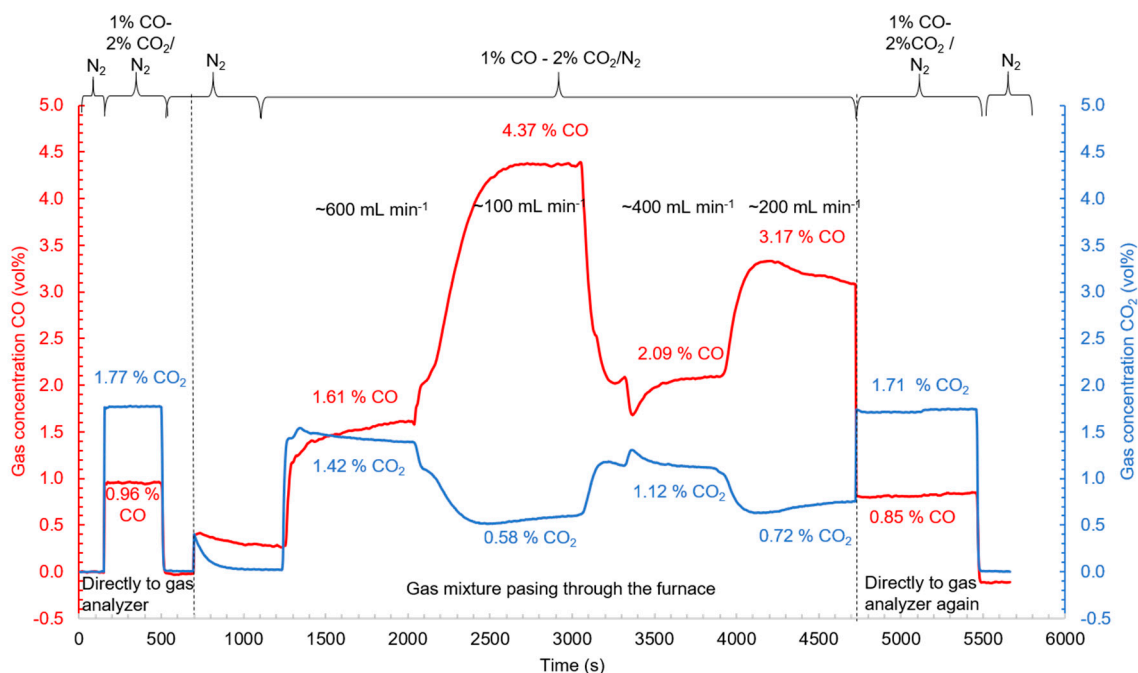


Figure 5. CO-CO<sub>2</sub> gas concentration in Setup 1.

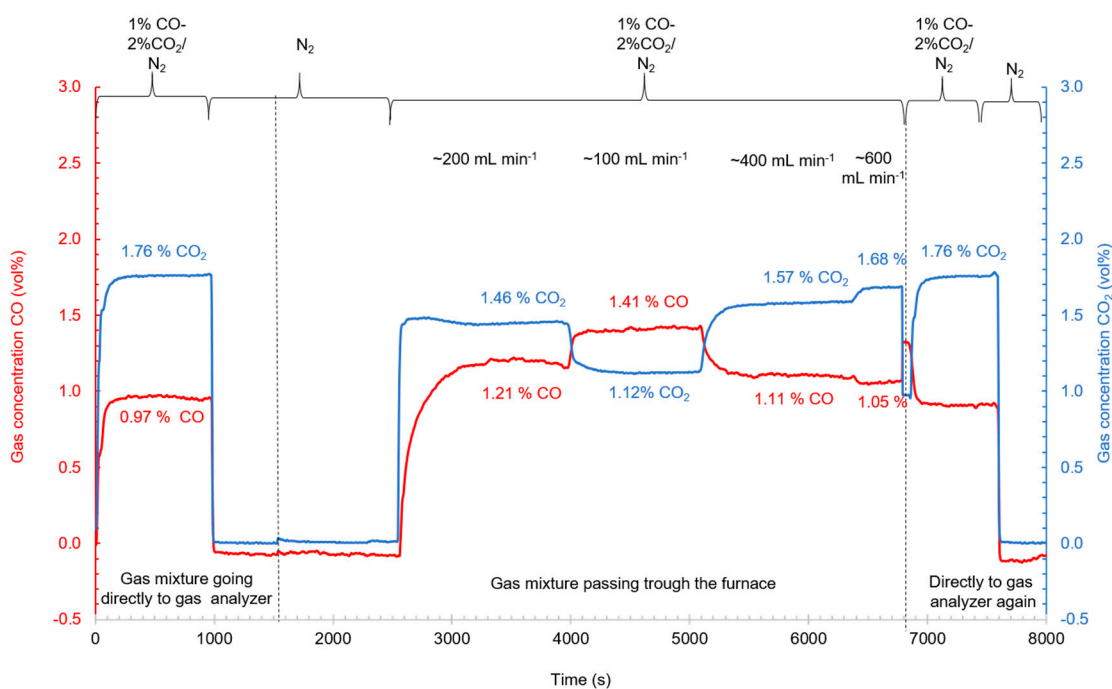
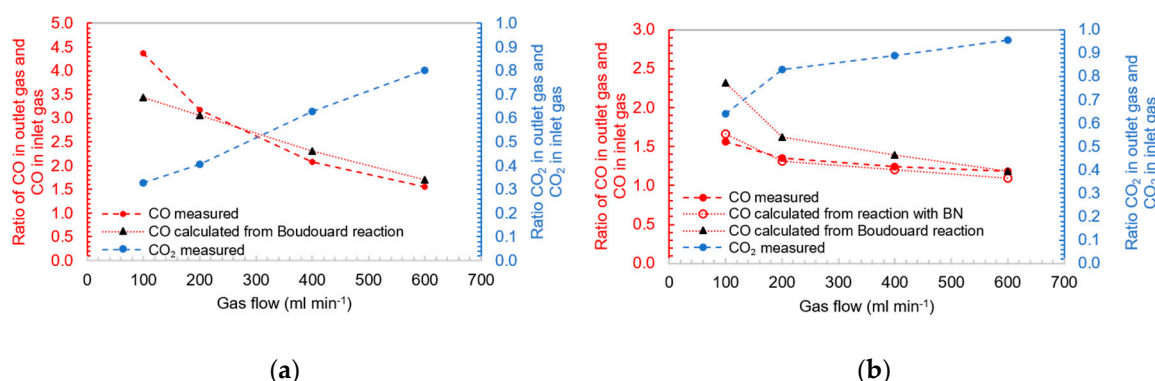


Figure 6. CO-CO<sub>2</sub> gas concentration in Setup 2.

There was an increase in CO concentration in the whole flow rate range compared against the inlet gas mixture. It was assumed that the Boudouard reaction is responsible for the CO<sub>2</sub> to CO conversion. At temperatures above 950 °C, CO is much more stable than CO<sub>2</sub>. The carbon crucible, rod anode and carbon plate in the bottom construction in Setup 1 are the sources of carbon. The CO concentration decreases with increasing gas flow while CO<sub>2</sub> gas concentration increases. This is most likely due to the increased time for reaction. If only the Boudouard reaction is responsible for the loss of CO<sub>2</sub> and corresponding CO concentration, it would give a CO<sub>2</sub> concentration of 3.34 vol% at the lowest flow rate.

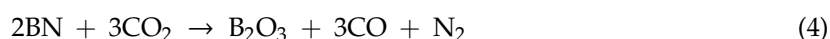
The measured concentration as shown in Figure 5 was 4.37 vol% CO. This excess of CO could indicate other reactions taking place besides the Boudouard reaction, as discussed below in relation to Figure 7.



**Figure 7.** The ratio of concentration in outlet gas and inlet gas for both CO and CO<sub>2</sub>: (a) Setup 1 and (b) Setup 2. For both setups, data indicated by red and blue solid circle markers represent measured CO and CO<sub>2</sub> concentration, respectively. Black triangular marker represents calculated CO concentration in outlet gas if CO<sub>2</sub> loss was only due Boudouard reaction. Non-filled red circle marker in (b) represents calculated CO concentration if CO<sub>2</sub> loss was only due to its reaction with BN.

The same CO(1%)/CO<sub>2</sub>(2%)/N<sub>2</sub>(balance) gas mixture was used for Setup 2 and the results are shown in Figure 6. When nitrogen was flushed through the analyzer and the furnace, the CO<sub>2</sub> concentration reached 0.00 vol% as expected, but the CO concentration reached −0.10 vol%. A separate test was done where nitrogen was flushed through the analyzer for 20 min and it was found that the CO<sub>2</sub> concentration remained stable (0.00 vol%) while the CO concentration reached −0.10 vol% and remained stable. This value was used later for the baseline correction. When the gas mixture was introduced, there was again observed a decrease in CO<sub>2</sub> and an increase in CO concentration, demonstrating some CO<sub>2</sub> to CO conversion but not to the same degree as for Setup 1. This is due to the absence of the graphite crucible as carbon source. The only carbon source in Setup 2 was the rod anode. The gas flow rate affected the gas composition in the same principal way as for Setup 1. At the highest flow rate, the CO<sub>2</sub> to CO conversion approaches zero. If it is assumed that all CO<sub>2</sub> loss was due to the Boudouard reaction, the calculated CO concentration becomes higher than the actually measured concentration at the lowest flow rate. The loss of the CO<sub>2</sub> could also be due to thermal decomposition taking place simultaneously with the Boudouard reaction.

Silny and Utigard [16] studied some factors which influence the CO/CO<sub>2</sub> ratio in primary gas composition and found that most of the CO was generated by CO<sub>2</sub> reacting with carbon particles arising from the disintegration of the carbon anode. They also found that CO<sub>2</sub> reacting with parts of boron nitride (BN) was a source for CO and they conducted some tests of the BN reactivity. They observed that CO<sub>2</sub> did not react with the BN in the absence of the bath, but when BN was immersed in the bath, CO<sub>2</sub> reacted with the BN, resulting in 17% CO in the outlet gas for that specific setup. Grjotheim et al. [18] also observed an excess of CO. In their gas measurements, helium was the carrier gas and it was found that the outlet gas always contained nitrogen. They estimated that boron nitride (which was used as construction material in the cell) probably reacted with CO<sub>2</sub> according to the reaction:



If it is assumed that in Setup 2, all CO<sub>2</sub> to CO conversion is due to reaction 4, the calculated concentration of CO is more in agreement with the obtained results in the test (Figure 7), meaning that in Setup 2, the boron nitride could be responsible for the conversion together with the Boudouard reaction. Sun et al. [19] found that CO<sub>2</sub> molecules form weak interactions with uncharged BN nanomaterials and are weakly adsorbed. When the BN is negatively charged CO<sub>2</sub> molecules become tightly bound

and strongly adsorbed. Once the electrons are removed from the BN, CO<sub>2</sub> molecules spontaneously desorb. From Figure 8, it can be seen that the reaction between BN and CO<sub>2</sub> is more thermodynamically favorable than the Boudouard reaction. Reaction between Si<sub>3</sub>N<sub>4</sub> and CO<sub>2</sub> could also be a source for CO, but it does not occur at the working temperature of 1005 °C.

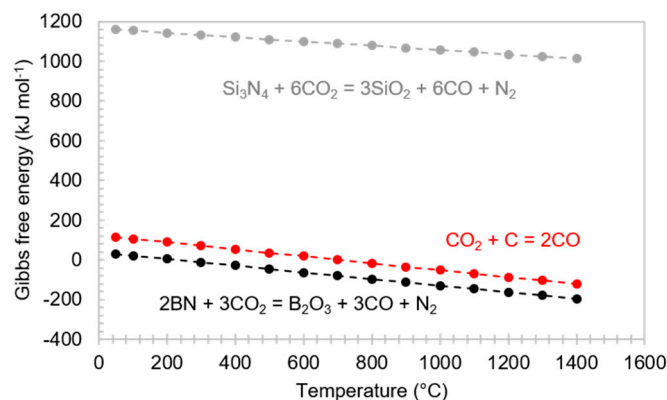


**Figure 8.** Gibbs free energy for the Boudouard reaction, CO<sub>2</sub> reacting with the boron nitride (BN) and Si<sub>3</sub>N<sub>4</sub> at various temperature.

Brun et al. [13] introduced a CO-CO<sub>2</sub> mixture of known amount and composition through a furnace in such a way that the gas mixture flowed past a graphite crucible which contained an alumina-saturated cryolite bath (12 wt% alumina) at an operating temperature of 1000 °C and no electrolysis took place. It was found that the amount of CO<sub>2</sub> leaving the furnace was only around 5% of the entering amount. They concluded that the Boudouard reaction proceeded rather rapidly.

As seen in Figures 5 and 6, the gas flow affects the gas concentration. Figure 7 shows the ratio of concentrations in outlet gas and inlet gas for both CO and CO<sub>2</sub> for both setups. Assuming that all loss of CO<sub>2</sub> was due to the Boudouard reaction, the corresponding CO concentration was calculated and is shown Figure 7. For Setup 1 (Figure 7a), the ratio agrees reasonably well with the calculated ratio except the lowest. The excess was approximately 1% CO. If humidity from the bath reacted with carbon according to reaction 5, the produced CO could explain the excess of CO in the outlet gas at the lowest flow rate.



If the excess was caused by reaction 5, it was calculated that the required mass of H<sub>2</sub>O should be ~0.2 g, corresponding to only 0.03 wt% of the total amount of cryolite in the crucible. Since the used cryolite has a purity of ≥ 97%, it could be possible that reaction 5 could affect the CO concentration.

For Setup 2 (Figure 7b), there is a deficit in CO assuming that the Boudouard reaction is the only conversion reaction for CO<sub>2</sub>. This means that there must be another conversion reaction for CO<sub>2</sub> taking place. However, the ratios approach each other towards higher flow rates. The only carbon source in Setup 2 is the rod anode. For Setup 2, it was also assumed another extreme case, i.e., all loss of CO<sub>2</sub> was due to reaction with BN. The ratio fits fairly well with the calculated ratios for all flow rates.

In the study of gas concentration obtained from the different anode designs, Setup 2 was used due to the smallest conversion of CO<sub>2</sub>. Although the conversion of CO<sub>2</sub> was lowest for the highest flow rate (600 mL min<sup>-1</sup>), the flow rate of 400 mL min<sup>-1</sup> was chosen as the dilution of the gas concentration was too large for the highest flow rate. At the flow rate of 400 mL min<sup>-1</sup>, the results from the test with Setup 2 showed that the actual CO<sub>2</sub> concentration is around 10% higher and the actual CO concentration is 20% lower than measured. The measured concentrations were corrected for these values.

### 3.2. Gas Measurements during Electrolysis

In Figure 9, (a) current response and (b) CO and CO<sub>2</sub> concentration for the rod anode at potential-controlled electrolysis are shown. A plot is shown for the whole potential range but also examples for two specific potentials (1.56 and 1.67 V) with corresponding current densities (0.07 and 0.2 A cm<sup>-2</sup>). Figures 10 and 11 summarize the results of many such experiments at different potentials obtained by plotting the anode potential and relative gas concentration as a function of the average current densities for the rod anode and inverted horizontal anode (Figure 10) and the horizontal anode and vertical anode (Figure 11). Some points for the gas measurements at very low potentials were not included if no significant change in gas concentration compared to open circuit condition could be measured. It can be seen that both the horizontal and vertical anode showed very high CO concentration in the whole potential range. This unlikely high CO concentration indicates that something failed during the experiment. An explanation for the results for these two electrodes is proposed.

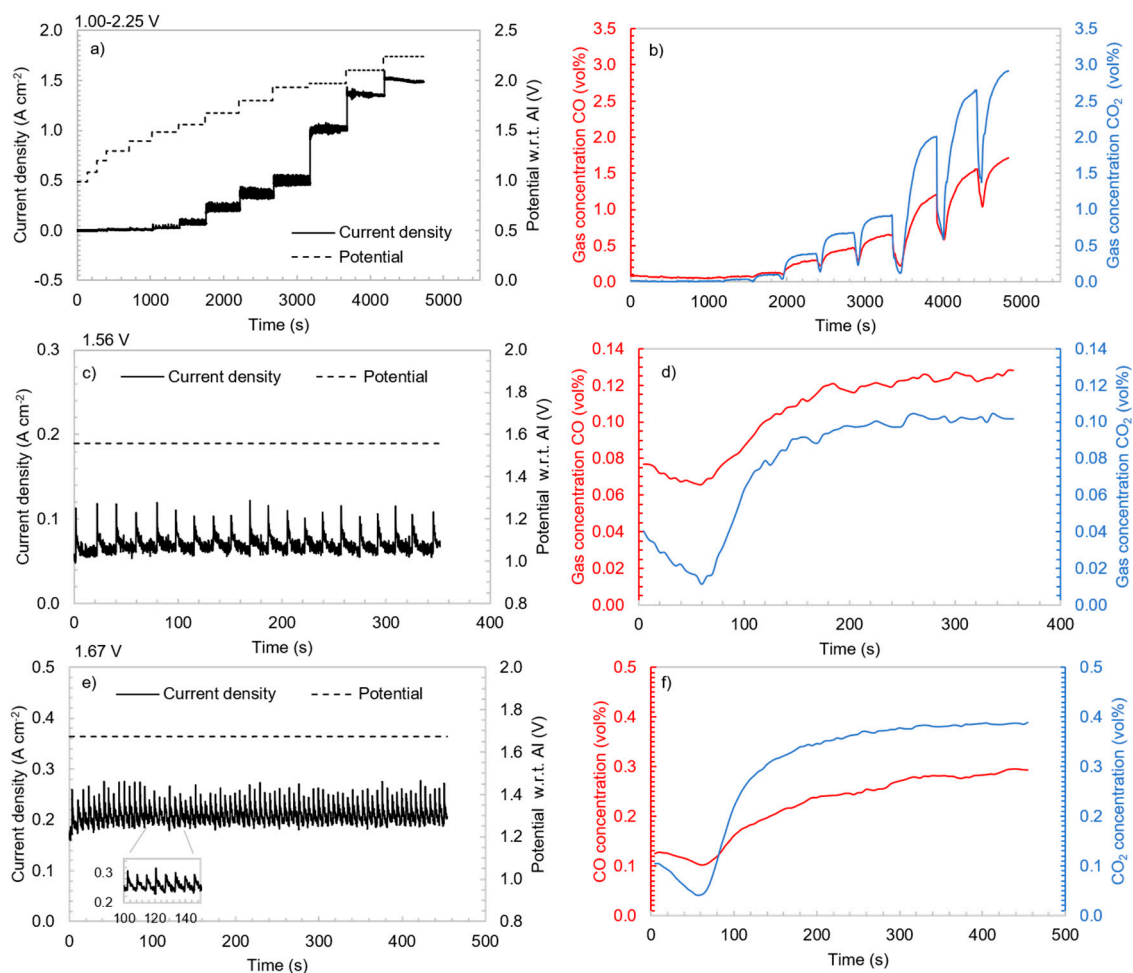


**Figure 9.** (a) Current response and (b) CO-CO<sub>2</sub> concentration for the rod anode at potential-controlled electrolysis in the potential range 1.00–2.25 V, (c) Current response and (d) CO-CO<sub>2</sub> concentration for the rod anode at constant potential of 1.56 V, (e) Current response and (f) CO-CO<sub>2</sub> concentration for the rod anode at constant potential of 1.67 V.

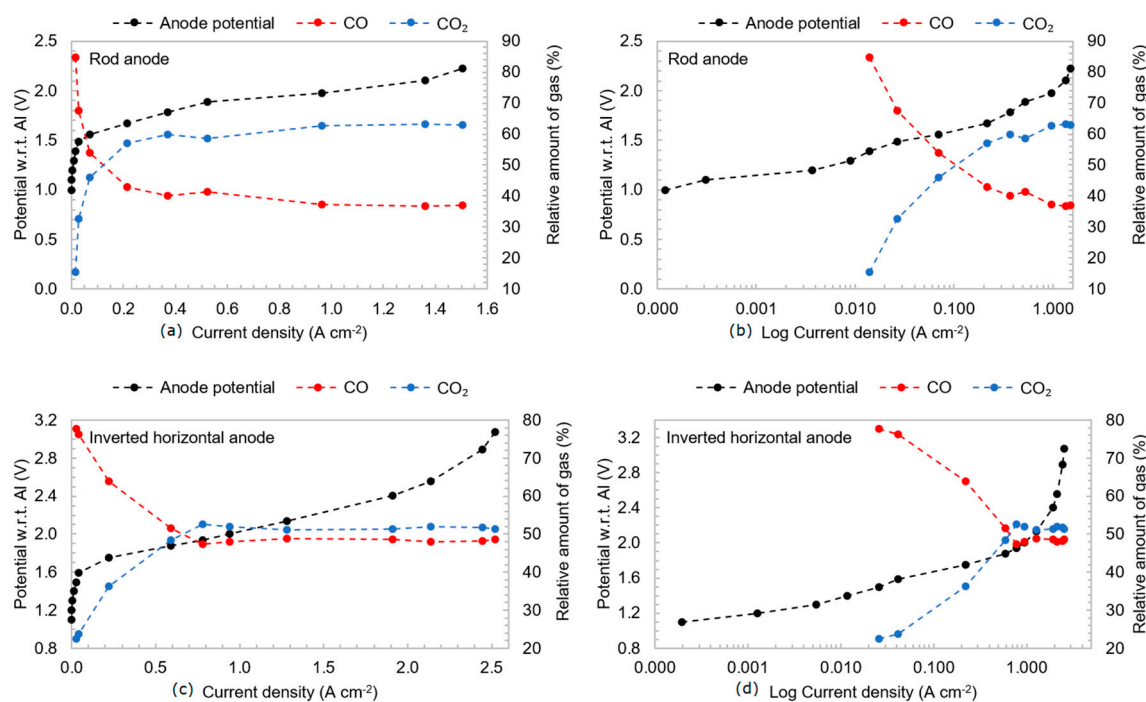


**Figure 10.** Anode potential and relative amount of the CO and CO<sub>2</sub> gas for the rod anode and inverted horizontal anode versus (a) current density (linear scale) for the rod anode, (b) current density (logarithmic scale) for the rod anode, (c) current density (linear scale) for the inverted horizontal anode and (d) current density (logarithmic scale) for the inverted horizontal anode.

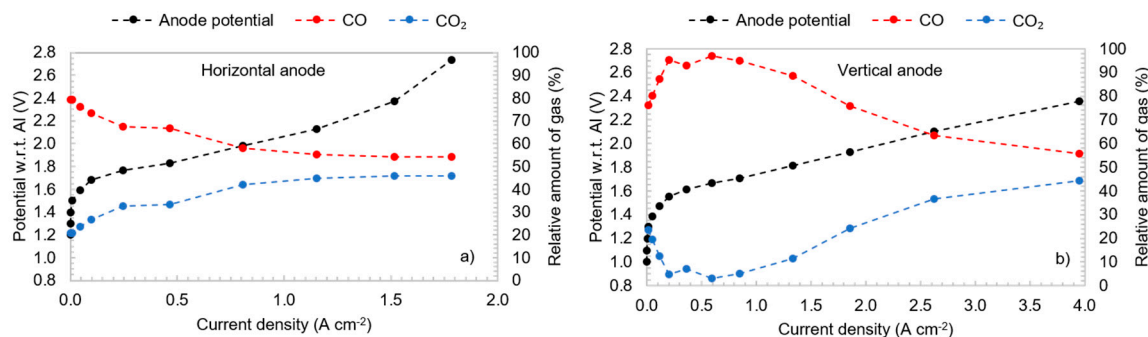


**Figure 11.** Anode potential and relative amount of the CO and CO<sub>2</sub> gas for the (a) horizontal anode and (b) vertical anode versus current density.

In Figures 10 and 11, it can be seen that at the potentials and current densities, the main anode gas is CO, which was also found by Thonstad [5]. Although the main constituent of the primary gas at higher current density should be CO<sub>2</sub>, a considerable amount of CO was also obtained. Due to the construction of the cell, it was assumed that the back reaction could not be the main source of formed CO at higher current densities. The main source of CO could be the Boudouard reaction between CO<sub>2</sub> and carbon particles in the melt. For high current densities, with the electrolysis taking place for some time, the anode can disintegrate, enabling the Boudouard reaction. After the experiment dusting was observed. The results from the rod anode are believed to be most trustable because the rod anode was the first electrode tested. After testing the rod electrode, the inverted horizontal anode was tested in the same bath. The bath might have contained carbon particles detached from the rod anode, thus converting through Boudouard reaction the CO<sub>2</sub> produced from the inverted horizontal anode.

Figure 12 shows images of the anodes after the experiment. Due to the long duration of the experiment, the anodes were considerably consumed and changed from their initial design.



**Figure 12.** Pictures of the anodes after the experiment: (a) rod anode, (b) horizontal anode, (c) vertical anode and (d) inverted horizontal anode (cross-sectioned).

Silny and Utigard [16] and Grjotheim [18] reported that the BN could play a significant role in  $\text{CO}_2$  to CO conversion (reaction 4). In Figure 13, can be seen that the edges of the BN shielding are still sharp. It is therefore concluded that the BN did not react with the  $\text{CO}_2$  as the edges then should be rather rounded. The reaction between  $\text{CO}_2$  and BN is therefore not a source for CO in the off-gas. Davies and Phennah [20] studied reactions of boron-containing materials with  $\text{CO}_2$  and found that, of all boron compounds, only BN showed a high degree of oxidation resistance in the temperature range 600–750 °C.



**Figure 13.** Images of anodes after experiment: (a) horizontal anode and (b) vertical anode.

As seen in Figure 11, a high CO concentration is obtained for the horizontal and vertical anode at all current densities. At higher current densities, graphite is considerably consumed (Figure 13) and the BN shielding hinders bubbles leaving the anode surface easily. Bubbles then will be stuck, increasing the contact time at the anode surface, thereby promoting  $\text{CO}_2$  to CO conversion. For the vertical anode at lower current densities, the behavior of the CO curve does not follow the decreasing trend observed for the other anodes (Figures 10 and 11). This could be explained by the wetting properties of graphite and BN by cryolite bath. Åsheim et al. [21] found that BN is better wetted by the cryolite in comparison to the graphite. For the vertical anode, produced gas can therefore become entrapped at the boundary between the graphite and the upper BN phase, as shown in Figure 14.

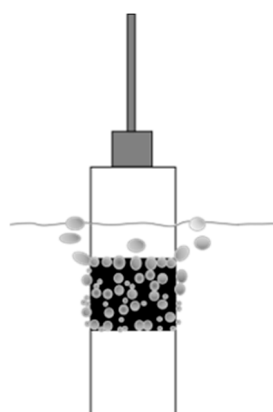


**Figure 14.** Illustration of entrapment of bubbles at the boundary between graphite and BN.

Chronoamperometric data for the horizontal anode were transformed to the frequency spectrum. Fast Fourier Transform (FFT) spectrum analysis was done using Sigview software. The FFT spectrum obtained for different current densities is shown in Figure A1 in Appendix A. The dominant frequency most likely represents the bubble release frequency for the horizontal anode. In Figure 15, the dominant frequency and how it changes with current density is shown. After longer electrolysis time, the graphite anode is considerably consumed and bubbles become trapped in the cavity, increasing the bubble retention time. In Figure 15, dominant frequencies for the horizontal anode where electrolysis time was much shorter, i.e., there was no cavity formation, are also shown. The dominant frequency for both anodes increases with increasing current density. From approximately  $0.5 \text{ A cm}^{-2}$ , there is a deviation for the anode having long electrolysis time, meaning that from this current density and upwards, the cavity formation severely affects the bubble retention time. Increased bubble retention time could have led to the generally high CO values at higher current densities.

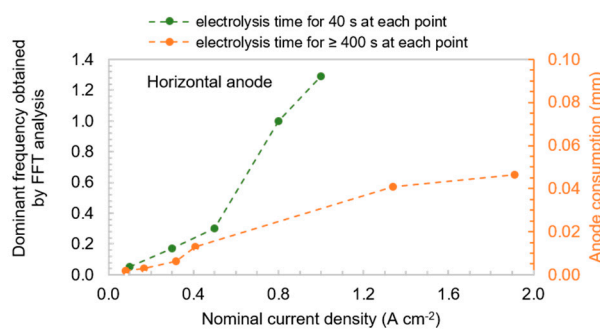


**Figure 15.** Dominant frequency obtained from FFT spectrum for the horizontal anode. Data for electrolysis time of 40 s are obtained from Stanic et al. [17].

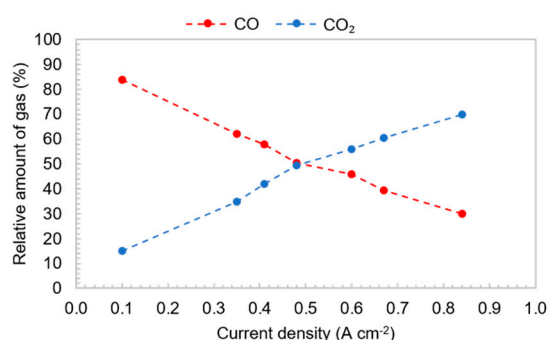
The carbon consumption for the rod, horizontal, vertical and inverted horizontal anode was calculated based on the measured volumetric consumption of the graphite and the results are shown in Table 1. The carbon consumption for the different anodes is comparable. If it is assumed that all CO for current densities above  $0.1 \text{ A cm}^{-2}$  comes from the Boudouard reaction, the corresponding calculated carbon consumption is in agreement with the carbon consumptions shown in Table 1 except for the rod anode. For the rod anode, it was found that only 50% of the consumed carbon had undergone Boudouard reaction. The remainder of the carbon remained in the melt as carbon particles. These carbon particles were also observed visually, as shown in Figure 16. The figure shows the bath surface in the silicon nitride crucible after the experiment. The density of the molten bath is around  $2.05 \text{ g cm}^{-3}$  and the density of the graphite is  $1.8 \text{ g cm}^{-3}$ , meaning that all carbon particles are found at the surface of the melt.

**Table 1.** Carbon consumption for the different anode designs.

Anode	Rod Anode	Horizontal Anode	Vertical Anode	Inverted Horizontal Anode
Carbon consumption %	126	130	134	117

**Figure 16.** Image of the surface of the frozen bath in the silicon nitride crucible at room temperature after the experiment with the rod anode and inverted horizontal anode.

In Figure 17, CO-CO<sub>2</sub> gas measurement results for the hollow gas anode from Figure 3 are shown. The experiments were conducted in the current range 0.10 to 0.85 A cm<sup>-2</sup>. The retention time (i.e., time until stabilization of gas concentrations) varied widely, for more than two hours at 0.10 A cm<sup>-2</sup> till three minutes at 0.85 A cm<sup>-2</sup>. The obtained CO concentration was higher than expected at higher current densities and could be explained by the Boudouard reaction taking place between produced CO<sub>2</sub> and carbon particles (formed by anode disintegration). The intersection of the CO and CO<sub>2</sub> curve could therefore be expected at lower current densities than obtained. Despite the long retention time at lower current densities, the hollow anode design performed reasonably well. Use of an inert carrier gas could lower the retention time; however, some challenges may arise in obtaining the product gas out due to overpressure in the cell.

**Figure 17.** Relative amount of CO and CO<sub>2</sub> versus current density for the hollow gas anode.

In general, the construction materials of the furnace were materials (stainless steel, pythagoras, sintered alumina, silicon-nitride) that could, to a small extent, react with the primary gases. Experimental conditions such as temperature and alumina concentration also can affect the primary gas concentration. Silny et al. [22] reported that increasing working temperature during electrolysis promotes the generation of CO relative to CO<sub>2</sub>. CO is always expected to be present at the temperature of the experiment due to the Boudouard reaction (reaction 2) [12]. Ouzilleau et al. [7] found that the

larger the crystallite diameter,  $L_a$  value, of the coke crystallites, the higher the  $\text{CO}_2$  fraction becomes. A single crystal of graphite would have an infinitely large  $L_a$  value. The graphite used in this work was not a single crystal but has seen much higher heat treatment than an industrial anode. In this way, it should give, according to Ouzilleau et al., more primary  $\text{CO}_2$ . The mentioned disintegration and following Boudouard reaction could have caused this effect. It has been reported by several researchers, although not documented quantitatively, that graphite disintegrates more than the industrial carbon anodes. Grjotheim et al. [11] observed a significant amount of carbon particles in the crucible after the experiment using the graphite anode. Thonstad [5] also reported that graphite anodes disintegrate more than industrial carbon anodes during electrolysis, inducing noticeable generation of CO by the reaction of carbon particles with  $\text{CO}_2$ .

$\text{CO}_2$  generated at the electrolytic surface of operating anodes permeates the porous anode structure and reacts to form carbon monoxide [23]. This gasification increases anode porosity and generates a reaction porosity profile. Far-Wharton et al. [24] studied gaseous reactions between  $\text{CO}_2$  and C at the electrode–electrolyte interface which occurs in the pore structure, giving rise to CO formation. The porosity of the carbon sample immediately behind the electrode–electrolyte interface was studied. An increasing proportion of CO evolution during electrolysis was associated with a greater amount of reactive carbon, which has a larger surface area and less developed crystallites. There is an increase in the number of macro-pores at high current density. The porosity of the anode surface at low current density ( $0.06 \text{ A cm}^{-2}$ ) increased while the porosity behind the electrode–electrolyte interface increased at higher current density. Putri et al. [25] used porosity measurement techniques to understand the relation between gas diffusion and anode properties. Two industrial anode samples and an anode made from graphite were tested. The graphite pore distribution was associated with a higher intrusion volume than the industrial anodes. According to these findings, it is reasonable to believe that any prolonged contact between  $\text{CO}_2$  and the anode itself, giving enough time for  $\text{CO}_2$  to penetrate the anode, would promote CO. After the reversible potential for  $\text{CO}_2$  formation is reached, this effect can influence the primary  $\text{CO}_2$ , especially when bubble retention time is extended due to, e.g., anode design, as in the case of the horizontal anode.

As stated above, the anodic current density, anode material, temperature and alumina content determine the CO- $\text{CO}_2$  gas concentration. In Figure 18, anode potentials and CO- $\text{CO}_2$  gas amounts are shown as a function of current density from previously reported works. The results from the current work obtained with the rod anode are also included. At potentials below 1.2 V (i.e., approx. the reversible potential for  $\text{CO}_2$  evolution), CO is the expected primary product. As seen in Figure 18b, Thonstad reported primary gas composition data from 1.05 V which show that the dominant primary off-gas was CO up to 1.2 V and  $0.15 \text{ A cm}^{-2}$ . Thonstad used a so-called non-disintegrating industrial anode which was supposed to give small dust amounts during electrolysis. Thonstad used a bath saturated with alumina. Alumina saturation is also used in several other works for simplicity regarding cell construction. Silny and Utigard [16] have also reported results for a non-saturated bath and found that decreasing alumina content promotes the evolution of CO. Two explanations were proposed for these observations. First, low alumina content results in higher overpotential for the anode process where  $\text{CO}_2$  is formed. It was not specified if this was related to concentration or reaction overpotential. Second, the interfacial tension increases with decreasing alumina content, which leads to lower wettability of the anode. This leads to larger gas bubbles and larger gas/anode interface area, which itself can promote the Boudouard reaction. However, this will also increase the local current density, which again can result in a higher dusting rate. Another explanation which can also account for the higher CO values at lower alumina concentration can be found in the structure of the oxyfluoro species. Sterten [26] developed an ionic structure model for NaF- $\text{AlF}_3$  melts containing alumina. There are two major species containing oxygen,  $\text{Al}_2\text{OF}_6^{2-}$  and  $\text{Al}_2\text{O}_2\text{F}_4^{2-}$ . At low alumina concentration, the dominant ion containing oxygen is  $\text{Al}_2\text{OF}_6^{2-}$ . Thus, steric effects could influence the reaction mechanism and thereby reaction rate and primary product. For the low oxygen-containing species ( $\text{Al}_2\text{OF}_6^{2-}$ ), the accessibility of oxygen for the surface carbon atoms is lower than for the high

oxygen-containing species ( $\text{Al}_2\text{O}_2\text{F}_4^{2-}$ ). The oxyfluoro complex containing two oxygen atoms could likewise promote primary  $\text{CO}_2$  formation. The relatively low alumina concentration (2 wt%) used in the current work could have given a slightly more primary  $\text{CO}$  than if the bath was saturated.

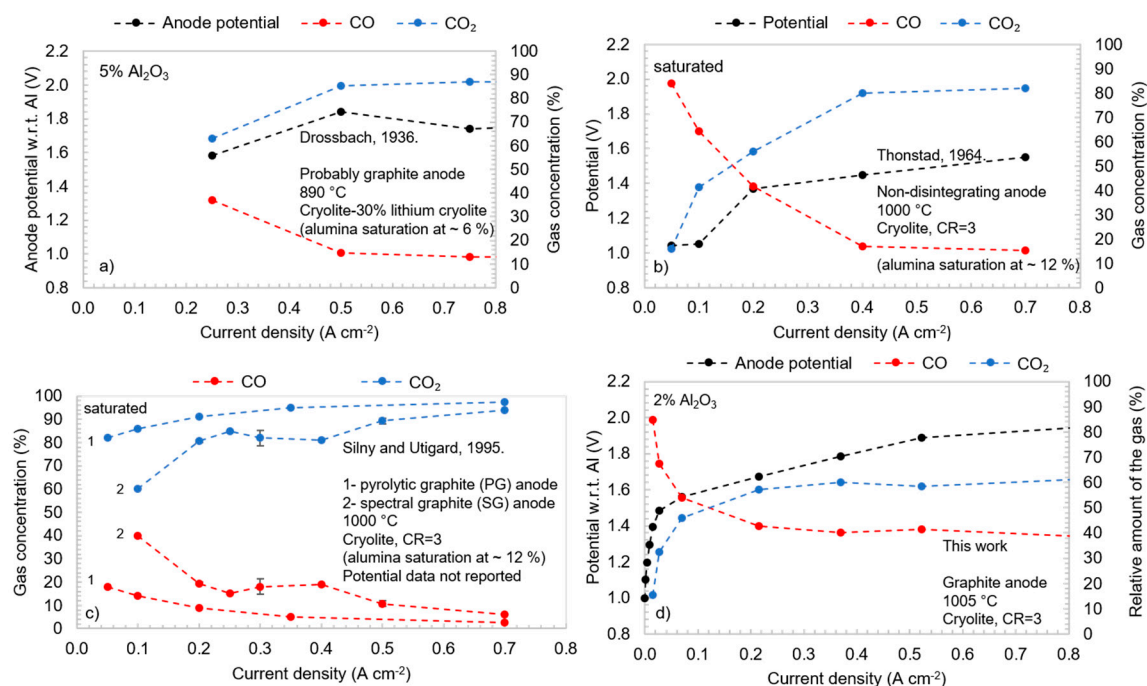


**Figure 18.** Anode potential and  $\text{CO}$  and  $\text{CO}_2$  amounts versus current density. (a) Data extracted from Thonstad [5], (b) Data extracted from Drossbach [15], (c) Data extracted from Silny and Utigard [16], (d) Data from this work (rod anode).

Drossbach measured the  $\text{CO}$ - $\text{CO}_2$  concentrations in a cryolite-lithium cryolite melt at  $890\text{ }^\circ\text{C}$  (Figure 18a). The starting point was at  $0.25\text{ A cm}^{-2}$ , where  $\text{CO}_2$  was already the dominant product. Values for lower current densities were not reported and  $\text{CO}$  was never found to be the dominant product, as Thonstad later found. At higher currents and potentials,  $\text{CO}_2$  is the dominant primary anode product, even though  $\text{CO}$  theoretically can be produced. The current perception is that reaction kinetics favor  $\text{CO}_2$  formation [5]. However, Drossbach showed that the thermodynamics actually can explain  $\text{CO}_2$  being the dominant primary gas product. Drossbach considered the equilibrium (reaction 6) and calculated gas composition ( $\text{CO}_2$ ,  $\text{CO}$ ,  $\text{O}_2$ ) for various potentials at  $890\text{ }^\circ\text{C}$ .



In Figure 19, the calculated  $\text{CO}$ - $\text{CO}_2$  gas concentrations as a function of anode potential are plotted. The thermodynamics predict  $\text{CO}$  to be the dominant gas species at low anode potentials, with an intersection somewhere in the interval 1.2 to 1.4 V.

Silny and Utigard (Figure 18c) found  $\text{CO}_2$  to be dominant in the whole current density range. Two different types of anode materials were used, spectral graphite (SG) and pyrolytic graphite (PG). Higher  $\text{CO}_2$  concentration was obtained for the PG anode. The SG anode tended to disintegrate and led to higher  $\text{CO}$  content than the PG anode due to  $\text{CO}_2$  reacting with the carbon particles from anode disintegration. PG has relatively few defects in its graphitic structure compared to the SG. Although this finding is not directly transferable to industrial anodes, Jentoftsen et al. [27] found that higher baking temperature probably leads to anodes dusting less. The used graphite material in the current work is probably closer in properties to the SG than the PG used by Silny and Utigard and partly can explain the observed disintegration.

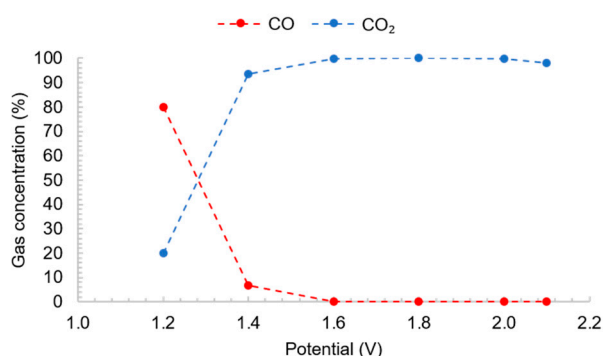


Figure 19. Drossbach's tabulated data plotted [15].

In the current work, the rod anode was the anode that gave lowest the CO concentration, especially at low potentials and low current densities but also at higher applied potentials in comparison to other anodes. The lowest applied anodic potential was 1.0 V, which gave a current density of  $0.1 \text{ mA cm}^{-2}$  but the first significant change in gas composition compared that at open circuit condition took place at 1.4 V and  $0.015 \text{ A cm}^{-2}$ . The dominant gas product was CO. The calculated theoretical value for the reversible potential of CO formation at this working temperature and alumina concentration (2 wt%) is approximately 1.1 V. Thonstad reported gas concentrations from 1.05 V and  $0.05 \text{ A cm}^{-2}$ . This is close to the reversible potential for CO formation at alumina saturation. A substantial amount of CO<sub>2</sub> (approx. 15%) was reported for this potential, even though the potential probably was below the reversible potential for CO<sub>2</sub> formation. In the current work, CO<sub>2</sub> becomes the dominant gas product approximately at 1.6 V and  $0.12 \text{ A cm}^{-2}$ , which is the intersection of the CO and CO<sub>2</sub> curve. The carbon particles found on the melt surface after the experiment indicate that anode carbon disintegration took place. This implies that the mentioned intersection could occur at an even lower current density than  $0.12 \text{ A cm}^{-2}$ .

#### 4. Conclusions

In the lower current density region  $0.015$  to  $0.07 \text{ A cm}^{-2}$ , CO was found to be the dominant anode gas product. Above 1.6 V and  $0.12 \text{ A cm}^{-2}$ , the dominant gas became CO<sub>2</sub>. Data extracted from Thonstad's work showed a lower potential but slightly higher current density. However, Thonstad used a saturated bath, making the results not directly comparable. Based on thermodynamic calculations presented by Drossbach, CO<sub>2</sub> starts to be the dominant gas product in the potential range 1.2 to 1.4 V. The relatively low alumina concentration of 2 wt% could have promoted higher primary CO content than in the saturated bath, explained by the favorable kinetics for CO formation through the steric effects of the different oxyfluoro-anion species that exist for different alumina concentrations. The carbon particles found on the melt surface after the experiment indicate that anode disintegration took place. The relatively high CO concentration at higher potentials and current densities was probably caused by the Boudouard reaction between CO<sub>2</sub> and carbon particles. The boron nitride used in the construction of the electrodes could, from a thermodynamic point of view, have reacted with CO<sub>2</sub> to form CO and boron oxide. Although stated by other authors to influence the CO-CO<sub>2</sub> gas concentration, this reaction seemed to have occurred to a very small degree because no wear of construction parts made of boron nitride was observed.

**Author Contributions:** N.S. performed all the experimental work with the rod, horizontal, vertical, inverted horizontal anode and wrote the manuscript with input from E.S., who supervised the work. N.S. designed the hollow gas anode and E.T.B. performed experimental work with Setup 3 and the hollow gas anode. All authors have read and agreed to the published version of the manuscript.

**Funding:** This research was funded by Norwegian University of Science and Technology. The APC was funded by Norwegian University of Science and Technology.

**Conflicts of Interest:** The authors declare no conflict of interest.

## Appendix A

Current density vs. time measurements were transformed into frequency spectra by using a Fast Fourier Transform algorithm in Sigview software for spectrum and signal analysis. The signals were transformed into the frequency domain to evaluate how the power of the signal is distributed over a range of frequencies to determine the dominant frequency for the horizontal anode. The dominant frequency most likely represents the bubble release frequency for the horizontal anode. The frequency spectrum is a simple way of showing the total amplitude at each frequency. The highest frequency that can be represented is one-half the sampling frequency, called the Nyquist frequency. The sampling rate ( $F_s$ ) was 5 Hz; consequently, the spectrum has a frequency range from zero to  $F_s/2$ , 0–2.5 Hz.

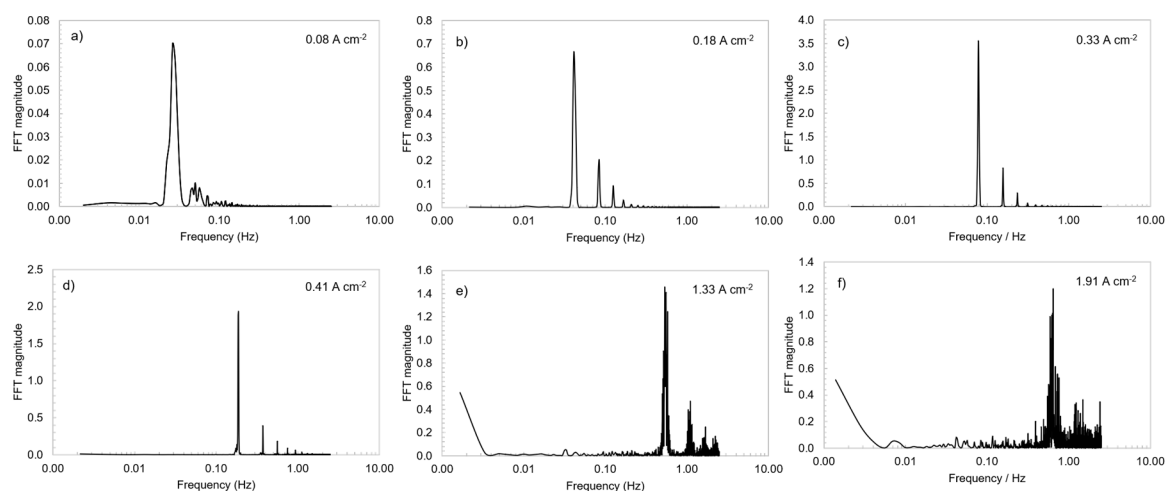


**Figure A1.** FFT spectrum of the current density–time data for the horizontal anode at different applied potentials. The current densities in the figure are the current densities measured in the moment the bubble has detached from the anode surface (i.e., the current obtained for the bubble-free surface): (a)  $0.08 \text{ A cm}^{-2}$ , (b)  $0.18 \text{ A cm}^{-2}$ , (c)  $0.33 \text{ A cm}^{-2}$ , (d)  $0.41 \text{ A cm}^{-2}$ , (e)  $1.33 \text{ A cm}^{-2}$ , and (f)  $1.91 \text{ A cm}^{-2}$ .

## References

- Thonstad, J.; Fellner, P.; Haarberg, G.M.; Híveš, J.; Kvande, H.; Sterten, Å. *Aluminium Electrolysis: Fundamentals of the Hall-Héroult Process*, 3rd ed.; Aluminium-Verlag: Düsseldorf, Germany, 2001; pp. 158–215.
- Thonstad, J. On the Anode Gas Reactions in Aluminum Electrolysis. *J. Electrochem. Soc.* **1965**, *111*, 955–959. [[CrossRef](#)]
- Kimmerle, F.M.; Noël, L.  $\text{CO}_2$ ,  $\text{CS}_2$  and  $\text{SO}_2$  Emissions from Prebaked Hall Héroult Cells. In *Light Metals 1997*; Huglen, R., Ed.; Minerals, Metals & Materials Society: Warrendale, PA, USA, 1997; pp. 153–158.
- Aarhaug, T.A.; Ferber, A.; Kjos, O.; Gaertner, H. Online Monitoring of Aluminium Primary Production Gas Composition by use of Fourier-Transform Infrared Spectroscopy. In *Light Metals 2014*; Grandfield, J., Ed.; Springer International Publishing: Cham, Switzerland, 2016; pp. 647–652.
- Thonstad, J. On the Anode Gas Reactions in Aluminum Electrolysis, II. *J. Electrochem. Soc.* **1965**, *111*, 959–965. [[CrossRef](#)]
- Barrillon, E. Les Facteurs de la Consommation de Carbone Anodique dans les Cuves Destinées à la Production Electrolytique de l'Aluminium. In Proceedings of the Travaux ICSOBA 3rd International Conference, Nice, France, 17–21 September 1973; pp. 691–700.
- Ouzilleau, P.; Gheribi, A.E.; Chartrand, P. Prediction of  $\text{CO}_2/\text{CO}$  formation from the (primary) anode process in aluminium electrolysis using an electrothermodynamic model (for coke crystallites). *Electrochim. Acta* **2018**, *259*, 916–929. [[CrossRef](#)]
- Novak, B.; Ratvik, A.P.; Wang, Z.; Grande, T. *Formation of Aluminium Carbide in Hall-Héroult Electrolysis Cell Environments*; Springer International Publishing: Cham, Switzerland, 2018; pp. 1215–1222.

9. Thorne, R.J.; Sommerseth, C.; Sandnes, E.; Kjos, O.; Aarhaug, T.A.; Lossius, L.P.; Linga, H.; Ratvik, A.P. Electrochemical Characterization of Carbon Anode Performance. In *Light Metals 2013*; Sadler, B., Ed.; Springer: Cham, Switzerland, 2013; pp. 1207–1211.
10. Kjos, O.S.; Aarhaug, T.A.; Skybakmoen, E.; Solheim, A.; Gudbrandsen, H. Fundamental Studies of Perfluorocarbon Formation. In Proceedings of the 10th Australasian Aluminium Smelting Technology Conference, Launceston, Tasmania, 9–14 October 2011.
11. Grjotheim, K.; Xiang, F.N.; Haugsdal, B.; Kvande, H. Current Efficiency Measurements in Laboratory Aluminium Cells—XI. Anode Gas Composition and Anode Consumption. *Can. Metall. Q.* **1987**, *26*, 181–184. [[CrossRef](#)]
12. Zhu, H.; Sadoway, D. An electroanalytical study of electrode reactions on carbon anodes during electrolytic production of aluminum. In *Light Metals: Proceedings of Sessions*; TMS: Warrendale, PA, USA, 2000; pp. 257–263.
13. Brun, M.; Thonstad, J.; Grjotheim, K.; Bratland, D. *A Study of the Effect of Cell Geometry, Bath Convection, and the Boudouard Equilibrium on the Operation of Laboratory Aluminum Cells: Preliminary Report*; The Metallurgical Society of ASME: Warrendale, PA, USA, 1979.
14. Sjøen, R.V. Anode Gas Measurement during Aluminium Electrolysis. Master's Thesis, NTNU, Trondheim, Sweden, 2019.
15. Droßbach, P. Zur Elektrometallurgie des Aluminiums. *Zeitschrift für Elektrochemie und Angewandte Physikalische Chemie* **1936**, *42*, 65–70.
16. Silny, A.; Utigard, T.A. Determination of the factors which control the CO/CO<sub>2</sub> ratio of the anode gas. In *Light Metals 1995*; Evans, J.W., Ed.; Minerals, Metals & Materials Society: Warrendale, PA, USA, 1995; pp. 205–211.
17. Stanic, N.; Jevremovic, I.; Martinez, A.M.; Sandnes, E. Bubble Evolution on Different Carbon Anode Designs in Cryolite Melt. *Metall. Mater. Trans. B* **2020**, *51*, 1243–1253. [[CrossRef](#)]
18. Grjotheim, K.; Malinovsky, M.; Matiašovský, K.; Silny, A.; Thonstad, J. Current efficiency measurements laboratory aluminum cells II. Influence of alumina content. *Can. Metall. Q.* **1972**, *11*, 295–298. [[CrossRef](#)]
19. Sun, Q.; Li, Z.; Searles, D.J.; Chen, Y.; Lu, G.; Du, A. Charge-Controlled Switchable CO<sub>2</sub> Capture on Boron Nitride Nanomaterials. *J. Am. Chem. Soc.* **2013**, *135*, 8246–8253. [[CrossRef](#)] [[PubMed](#)]
20. Davies, M.; Phennah, P. Reactions of Boron Carbide and Other Boron Compounds with Carbon Dioxide. *J. Appl. Chem.* **1959**, *9*, 213–219. [[CrossRef](#)]
21. Åsheim, H.; Eidsvaag, I.A.; Solheim, A.; Gudbrandsen, H.; Haarberg, G.M.; Sandnes, E. The Influence of Polarisation on the Wetting of Graphite in Cryolite-Alumina Melts. In *Light Metals*; Springer International Publishing: Cham, Switzerland, 2020; pp. 608–619.
22. Silny, A.; Korenko, M.; Daneck, V.; Chrenkova, M. Carbon Consumption during Laboratory Aluminium Electrolysis. *Can. Metall. Q.* **2006**, *45*, 275–282. [[CrossRef](#)]
23. Sadler, B.; Algie, S. A Porosimetric Study of Sub-Surface Carboxy Oxidation in Anodes. In *Essential Readings in Light Metals*; Johnson, J.A., Tomsett, A., Eds.; Springer: Cham, Switzerland, 2013; pp. 594–605.
24. Farr-Wharton, R.; Welch, B.J.; Hannah, R.C.; Dorin, R.; Gardner, H.J. Chemical and electrochemical oxidation of heterogeneous carbon anodes. *Electrochim. Acta* **1980**, *25*, 217–221. [[CrossRef](#)]
25. Putri, E.; Brooks, G.; Snook, G.; Eick, I. Anode characterisation and gas diffusion behaviour in aluminium smelting. In *AIP Conference Proceedings 1805*; AIP Publishing: Bandung, Indonesia, 2017; p. 040001-1-9.
26. Sterten, Å. Structural entities in NaF AlF<sub>3</sub> melts containing alumina. *Electrochim. Acta* **1980**, *25*, 1673–1677. [[CrossRef](#)]
27. Jentoftsen, T.E.; Linga, H.; Holden, I.; Aga, B.E.; Christensen, V.G.; Hoff, F. Correlation between Anode Properties and Cell Performance. In *Light Metals 2009*; Bearne, G., Ed.; Minerals, Metals & Materials Society: Warrendale, PA, USA, 2009; pp. 301–304.

**Publisher's Note:** MDPI stays neutral with regard to jurisdictional claims in published maps and institutional affiliations.



© 2020 by the authors. Licensee MDPI, Basel, Switzerland. This article is an open access article distributed under the terms and conditions of the Creative Commons Attribution (CC BY) license (<http://creativecommons.org/licenses/by/4.0/>).